

# Simple and High-Yield Preparation of Carbon-Black-Supported ~1-nm Platinum Nanoclusters and Their Oxygen Reduction Reactivity

Tokuhisa Kawawaki,<sup>‡,1</sup> Nobuyuki Shimizu,<sup>‡,1</sup> Kanako Funai,<sup>1</sup> Yusuke Mitomi,<sup>1</sup> Sakiat Hossain,<sup>1</sup> Soichi Kikkawa,<sup>2</sup> D. J. Osborn,<sup>3</sup> Seiji Yamazoe,<sup>2</sup> Gregory F. Metha,<sup>3</sup> and Yuichi Negishi<sup>\*1</sup>

<sup>1</sup> Department of Applied Chemistry, Faculty of Science, Tokyo University of Science, Kagurazaka, Shinjuku-ku, Tokyo 162-8601 (Japan), E-mail; negishi@rs.tus.ac.jp

<sup>2</sup> Department of Chemistry, Graduate School of Science, Tokyo Metropolitan University, 1-1 Minami-Osawa, Hachioji-shi, Tokyo 192-0397 (Japan)

<sup>3</sup> Department of Chemistry, University of Adelaide, Adelaide, South Australia 5005 (Australia)

<sup>‡</sup> These authors contributed equally

## 1. Chemicals

All chemicals were commercially obtained and used without further purification. Hydrogen hexachloroplatinate hexahydrate (H<sub>2</sub>PtCl<sub>6</sub>·6H<sub>2</sub>O) was obtained from Tanaka Kikinok. Sodium hydroxide (NaOH), *n*-octanethiol, Pt standard solution (1000 mg/L), bismuth standard solution (100 ppm), and perchloric acid (HClO<sub>4</sub>) were obtained from FUJIFILM Wako pure Chemical Co.. Methanol, 2-propanol, toluene, ethylene glycol, dichloromethane, hydrochloric acid, and nitric acid (HNO<sub>3</sub>) were obtained from Kanto Kagaku. Carbon Black (CB; Vulcan<sup>®</sup> XC-72), which was dried under vacuum before usage, was purchased from Fuel Cell Earth. CB-supported Pt nanoparticles (Pt<sub>NP</sub>/CB; EC-10-PTC) was purchased from Toyo Co.. 2-Phenylethanethiol and Nafion<sup>®</sup> defluorinated resin solution were obtained from Sigma Aldrich. *trans*-2-[3-(4-*tert*-Butylphenyl)-2-methyl-2-propenylidene]malononitrile (DCTB) was purchased from Tokyo Kasei. Pure Milli-Q water (>18 MΩ·cm) was generated using a Merck Millipore Direct 3 UV system.

## 2. Synthesis and Preparation

### 2.1. Synthesis of Ligand-protected Pt<sub>-35</sub> (1), Pt<sub>-51</sub> (2), and Pt<sub>-66</sub> (3) NCs

Pt NC, **1**, **2**, or **3**, was synthesized by polyol reduction using ethylene glycol (Figure S4 and S5), similar to our previous study on triphenylphosphine-protected Pt<sub>17</sub> nanocluster ([Pt<sub>17</sub>(PPh<sub>3</sub>)<sub>8</sub>(CO)<sub>12</sub>]<sup>2+</sup>; z = 1, 2).<sup>1,2</sup> First, NaOH (225 mM) was dissolved in ethylene glycol (15 mL). Then, 0.20 mmol of H<sub>2</sub>PtCl<sub>6</sub>·6H<sub>2</sub>O was added to this solution. The solution was heated at 80 °C for 15 min, and then heated at 120 °C to reduce Pt ions into atoms in the solution. After ~2 min of heating at 120 °C, the color of the solution changed from orange to dark brown. After heating for a specific period (4 min for **1**, 30 min for **2**, and 120 min for **3**), the solution was rapidly cooled in an ice bath from 120 °C to room temperature (~25 °C) within ~1 min. The mixture of 2-phenylethanethiol (2.0 mmol) and toluene (5 mL) was then added to this solution and the solution was stirred at room temperature for 1 hour. After stirring, ~15 mL of water was added to the solution, and hydrophilic unreacted species and byproducts were removed by separating the aqueous layer by centrifugation. The obtained organic phase was dried by rotary evaporator and then washed with water and then methanol to remove impurities (*i.e.* unreacted thiol). The objective **1**, **2**, or **3** was extracted from the precipitate by toluene.

### 2.2. Preparation of Pt<sub>-35</sub>/CB, Pt<sub>-51</sub>/CB, and Pt<sub>-66</sub>/CB Catalysts

Each Pt<sub>-*n*</sub> was loaded on CB using the following method. First, **1**, **2**, or **3** was adsorbed onto CB by mixing **1**, **2**, or **3** with CB (60 mg) in 30 mL of toluene solution for 18 h at room temperature. The solution became almost transparent when **1**, **2**, or **3** was dissolved at a ratio of 1.0 wt % Pt. The CB includes 6-membered carbon rings in the framework structure;<sup>3</sup> thus, a π-π interaction was expected to occur between these functional groups and the phenyl group of PET. In addition, CB also contains hydroxyl groups and carboxyl groups;<sup>3</sup> thus, hydrogen bonds were expected to form between these polar functional groups and CO. It can be interpreted that **1-3** was adsorbed on the CB with a high adsorption rate when mixed at a weight ratio of 1.0 wt% Pt because of these two interactions. In contrast, the solution remained colored when **1**, **2**, or **3** was dissolved at an adsorption ratio of 10.0 wt % Pt. The amount of Pt adsorbed onto CB was exactly determined by measuring the quantities of Pt in solution before and after the adsorption by an inductively coupled plasma mass spectrometry (ICP-MS) (Table S6).<sup>2</sup> The resulting powder (CB adsorbed by **1**, **2**, or **3**) was then calcined in an electric furnace under reduced pressure (~1.0 × 10<sup>-1</sup> Pa) to remove most of the ligands. For this calcination, the temperature was increased at a rate of 5 °C/min and maintained at 200 °C for 20 min.

### 2.3. Preparation of Catalyst Slurry

To conduct the electrochemical measurement for Pt<sub>-35</sub>/CB, Pt<sub>-51</sub>/CB, Pt<sub>-66</sub>/CB, and commercial Pt<sub>NP</sub>/CB, the catalyst slurry was prepared as follows. First, 12 mg of catalyst powder (Pt<sub>-35</sub>/CB, Pt<sub>-51</sub>/CB, Pt<sub>-66</sub>/CB, or commercial Pt<sub>NP</sub>/CB) was dispersed in the solution containing 2.0 mL of H<sub>2</sub>O and 0.5 mL of 2-propanol. Then, 10 μL of Nafion<sup>®</sup> solution was added to this solution. The vial containing this mixture was sealed and then ultrasonicated for 30 min in an ice bath (Figure S23a).

## 3. Characterization

The transmission electron microscope (TEM) images were recorded with a H-9500 electron microscope (HITACHI, Tokyo, Japan) or JEM-2100 electron microscope (JEOL, Tokyo, Japan) operating at 200 kV, typically using magnification of 600 000.

The high-angle annular dark field scanning TEM (HAADF-STEM) images were obtained by ultra-high-resolution transmission electron microscope (The FEI Titan Themis 80–200) operating at 200 kV, with a beam convergence semi angle of 25 mrad and HAADF collection angle from 56–200 mrad. Elemental maps were acquired using a super X detector and low-background sample holder.

Pt L<sub>3</sub>-edge X-ray absorption fine structure (XAFS) measurements were performed at beamline BL01B1 of the SPring-8 facility of the Japan Synchrotron Radiation Research Institute (proposal numbers 2020A0695, 2020A1410 and 2020A1219). The incident X-ray beam was monochromatized by a Si(111) double-crystal monochromator. As references, XAFS spectra of Pt foil and solid PtO<sub>2</sub> were recorded in transmission mode using ionization chambers. The Pt L<sub>3</sub>-edge XAFS spectra of the samples were measured in fluorescence mode using a 19-element Ge solid-state detector at room temperature. The X-ray energies for the Pt L<sub>3</sub>-edges were calibrated using Pt foil. The XANES and EXAFS spectra were analyzed using xTunes<sup>4</sup> as follows. The  $\chi$  spectra were extracted by subtracting the atomic absorption background using cubic spline interpolation and normalized to the edge height. The normalized data were used as the XANES spectra. The  $k^3$ -weighted  $\chi$  spectra in the  $k$  range 3.0–14.0 Å<sup>-1</sup> for the Pt L<sub>3</sub>-edge were Fourier transformed into  $r$  space for structural analysis.

The Pt 4f and sulfur (S) 2p X-ray photoelectron spectroscopy (XPS) spectra were collected by using a JPS-9010MC electron spectrometer (JEOL, Tokyo, Japan) at a base pressure of  $\sim 2 \times 10^{-8}$  Torr. X-rays from the Mg-K $\alpha$  line (1253.6 eV) were used for excitation. Each NCs was deposited on an Ag plate and the spectra were calibrated with the peak energies of Ag 3d<sub>5/2</sub> (368.22 eV).

The ultraviolet-visible (UV-vis) absorption spectra of products were acquired in dichloromethane solution at room temperature with a V-630 spectrometer (JASCO, Tokyo, Japan).

Fourier transform infrared (FT-IR) spectra of the product were obtained using the attenuated total reflectance (ATR) method in the region between 400 and 4000 cm<sup>-1</sup> by a FT/IR-4600-ATR-PRO ONE spectrometer (JASCO, Tokyo, Japan) equipped with a DLATGS detector as the average of 50 scans at 4 cm<sup>-1</sup> resolution.

The matrix assisted laser desorption/ionization (MALDI) mass spectra were recorded with a JMS-S3000 spiral time-of-flight mass spectrometer (JEOL, Tokyo, Japan) equipped with a semiconductor laser ( $\lambda = 349$  nm). DCTB was used as the MALDI matrix. To minimize NC dissociation induced by laser irradiation, the NC-to-matrix ratio was fixed at 1:1000.

Thermogravimetric analysis (TGA) was performed with a TGA2000SA (Bruker, Massachusetts, USA) and at a heating rate of 5 °C min under a nitrogen (N<sub>2</sub>) atmosphere to 900 °C from room temperature.

TG-MS was performed with an STA 2500 Regulus (NETZSCH, Bavaria, Germany) and a JMS-Q 1500GC (JEOL, Tokyo, Japan) at a heating rate of 5 °C min under a He atmosphere over the temperature range of 40–900 °C.

ICP-MS was performed with an Agilent 7500c spectrometer (Agilent Technologies, Tokyo, Japan). Bismuth was used as the internal standard. The ICP-MS measurements were performed for the solution before and after mixing 1–3 with CB to estimate the adsorbed or loaded Pt content.

#### 4. Electrochemical measurement

All electrochemical measurements were performed using a CHI 710D electrochemical work-station (ALS, Osaka, Japan) with a RRDE-3A rotating ring disk electrode apparatus (BAS, Tokyo, Japan). A rotating disk electrode (RDE,  $\phi = 5$  mm) was polished with diamond paste and alumina paste and then sonicated in water before the usage. A counter electrode, Pt ring electrode, was cleaned by a sonication in 10% HNO<sub>3</sub> before the usage. Silver-silver chloride (Ag/AgCl) electrode was used as reference electrode. In the setup, first, the catalyst slurry prepared using the method described in section 2.2.3 was sonicated in ice bath for 30 min and then 10  $\mu$ L of the catalyst slurry was carefully dropped onto RDE by spin-coat method (Figure S23a).<sup>5</sup> After the catalyst slurry was dried enough, each electrode was set into electrochemical measurement system containing 0.10 mol/L of HClO<sub>4</sub> solution (pH = 1.0) as electrolyte (Figure S23b).

In the measurements, N<sub>2</sub> gas was first bubbled for 30 min and then cyclic voltammetry (CV) was conducted 100 times in the region from -0.016 V to 1.254 V (vs. reversible hydrogen electrode; RHE) with a scanning rate of 200 mV/s for the cleaning of the electrodes.<sup>5</sup> Thereafter, CV was performed 3 times in the region from -0.016 V to 1.000 V (vs. RHE) with the rate of 20 mV/s to evaluate ECSA. After CV, a linear sweep voltammetry (LSV) was performed under N<sub>2</sub> atmosphere in the region from 0.000 V to 1.000 V (vs. RHE) with the rate of 10 mV/s. Then, LSV was performed under oxygen (O<sub>2</sub>) gas atmosphere in the region from 0.000 V to 1.000 V (vs. RHE) with the rate of 10 mV/s while rotating RDE at the rate of 400, 900, 1600, 2500 rpm (Figure S24 and S25).

In the durability test, a cleaning of the electrodes was initially undertaken. Then, CV was performed 3 times in the region from -0.016 V to 1.000 V (vs. RHE) with scanning rate of 20 mV/s to evaluate ECSA. This value was used as ECSA of the sample before durability test. Thereafter, the catalyst was kept under the potential of 1.000 V (vs. RHE) for 30 sec and then exposed to the repeated CV sweep in the region from 1.000 to 1.500 V (vs. RHE) at the rate of 500 mV/s. This repeated CV sweep was performed until the ECSA value fell down below 50% of the initial value (Figure S32 and S33).<sup>6</sup>

#### 5. Analysis

##### 5.1. Estimation of Chemical Composition for 1–3

Assuming that in the MALDI-MS spectrum of 1–3 the peaks attributed to Pt<sub>*n*</sub>S<sub>*m*</sub>(CO)<sub>*l*</sub> are caused by S–C bond dissociation (Figure S12 and S13), we explored the combination of  $n$ ,  $m$ , and  $l$  attributed to the strongest peak in the MALDI-MS spectrum (Figure 3a). The weight ratio of Pt, PET, and CO calculated for Pt<sub>*n*</sub>(PET)<sub>*m*</sub>(CO)<sub>*l*</sub> using the obtained the combination of  $n$ ,  $m$ , and  $l$  was constrained so that it was consistent with the result of the TGA (Figure 3b): the weight loss in the range of 160–300 °C is equivalent to the weight of PhC<sub>2</sub>H<sub>4</sub> caused by the S–C bond dissociation (Figure S14), that in the range of 750–900 °C corresponds to the weight of S and CO (Figure S14), the residual weight at 900 °C corresponds to the weight of Pt (Table S2). Considering the experimental error, we searched for combinations of  $n$ ,  $m$ , and  $l$  with a width of  $\pm 5$  Da for the mass-to-charge ratio ( $m/z$ ) and  $\pm 2\%$  for TGA curve. As a result, only the chemical compositions shown in Table S3–5 didn't contradict with the results of MALDI-MS and TGA. Although this is a rough estimation,

considering the results obtained for Au<sub>25</sub>(SR)<sub>18</sub>,<sup>7,8</sup> Au<sub>38</sub>(SR)<sub>24</sub>,<sup>9,10</sup> and Au<sub>144</sub>(SR)<sub>60</sub><sup>11,12</sup> (SR = alkanethiolate or PET) the number of Pt atoms calculated on this assumption seems to reflect the actual value relatively well.

## 5.2. Estimation of Particle Size of Pt Core for 1–3

The following equation was used in the calculation of the particle diameter ( $D$ ; nm) of Pt core using the density of bulk Pt for 1–3:

$$D = \sqrt[3]{\frac{6nM}{\pi\rho N_A}} \times 10^7 \quad (1)$$

where  $n$  is the number of Pt atoms estimated from MALDI-MS and TG-MS results (Table S3–5),  $\pi$  is circular constant (3.14),  $\rho$  is the density of bulk Pt (21.45 g cm<sup>-3</sup>),  $N_A$  is Avogadro constant (6.02 × 10<sup>23</sup> mol<sup>-1</sup>), and  $M$  is the atomic weight of Pt (195.1 g mol<sup>-1</sup>).

## 5.3. Estimation of the Number of Transferred Electrons for Each Catalyst at Diffusion-Limited Region and Mass Activity.

These values are estimated using the Koutecky-Levich equation;<sup>13,14</sup>

$$\frac{1}{I} = \frac{1}{I_k} + \frac{1}{I_d} = \frac{1}{I_k} + \frac{1}{0.62nFACD^{2/3}\nu^{-1/6}\omega^{1/2}} \quad (2)$$

where  $I_k$  is kinetic current,  $I_d$  is diffusion limiting current,  $n$  is the number of transfer electrons,  $F$  is Faraday constant,  $A$  is geometric area of electrode,  $C$  is concentration of O<sub>2</sub> in the electrolyte (1.26 × 10<sup>-6</sup> mol/cm<sup>3</sup>),  $D$  is diffusion coefficient of O<sub>2</sub> (1.93 × 10<sup>-5</sup> cm<sup>2</sup>/s),  $\nu$  is viscosity of the electrolyte (1.0 × 10<sup>-2</sup> cm<sup>2</sup>/s), and  $\omega$  is angular rotation speed of the electrode. Mass activity is obtained from  $I_k$  by dividing the measured current by geometric area of electrode ( $A$ ) and loading weight of Pt (Figure S26 and S27).

## 6. Additional Tables

**Table S1. Possible Assignments of Peaks Observed in FT-IR Spectra**

Wavenumber (cm <sup>-1</sup> )			Assignment <sup>a</sup>
Pt-35	Pt-51	Pt-66	
3059.5	3057.6	3058.5	v(C-H) phenyl
3026.7	3026.7	3027.7	v(C-H) phenyl
2954.1	2956.3	2957.3	v(C-H) ethyl
2922.6	2923.6	2924.5	v(C-H) ethyl
2850.3	2855.1	2854.1	v(C-H) ethyl
2012.4, 2003.4	2008.5, 1997.9	2008.5, 2001.7	terminal CO
1783.8	1781.9	1784.8	bridge CO
1600.6	1600.6	1600.6	v(C-C) phenyl
1493.6	1492.6	1492.7	v(C-C) phenyl
1447.3	1455.0	1448.3	v(C-C) phenyl or ethyl
1268.9	1263.2	1270.9	δ(C-H) phenyl or ethyl
1026.9	1030.8	1028.8	δ(C-H) phenyl
911.2	907.3	908.7	δ(C-H) phenyl
756.0	729.9	756.0	δ(C-H) phenyl
702.0	696.2	701.0	δ(C-H) phenyl

<sup>a</sup> See Reference 15–18.

**Table S2. Ratio of the Number of Pt, PET, and CO in 1–3 Estimated from TGA Curves and TG-MS Analyses**

NC	Pt <sup>a</sup>	PET <sup>a</sup>	CO <sup>a</sup>
1	1	1.08	0.63
2	1	0.69	0.13
3	1	0.61	0.13

<sup>a</sup> See Figure 3b and Figure S14. In the table, the value of Pt is fixed to 1.

**Table S3. Possible Assignments for the Strongest Peak Observed in MALDI-MS Spectrum of 1**

Calculated Molecular Weight (Da)	The number of atoms or molecules		
	Pt ( $n$ )	S ( $m$ )	CO ( $l$ )
8483.4	34	35	26
8487.4	34	36	25
8486.5	35	36	18
8485.8	36	43	3

**Table S4. Possible Assignments for the Strongest Peak Observed in MALDI-MS Spectrum of 2**

Calculated Molecular Weight (Da)	The number of atoms or molecules		
	Pt ( $n$ )	S ( $m$ )	CO ( $l$ )
11343.6	51	33	12
11347.6	51	34	11
11343.9	51	40	4
11342.6	52	33	5
11346.6	52	34	4

**Table S5. Possible Assignments for the Strongest Peak Observed in MALDI-MS Spectrum of 3**

Calculated Molecular Weight (Da)	The number of atoms or molecules		
	Pt ( <i>n</i> )	S ( <i>m</i> )	CO ( <i>l</i> )
14430.1	66	38	12
14434.2	66	39	11
14438.2	66	40	10
14429.1	67	38	5
14433.2	67	39	4
14437.3	67	40	3

**Table S6. Relation between Amount of Pt in Starting Solution, Adsorption Rate, and Amount of Pt Loaded on CB**

Cluster	Pt <sub>-35</sub>		Pt <sub>-51</sub>		Pt <sub>-66</sub>	
	without calcination	after calcination	without calcination	after calcination	without calcination	after calcination
Amount of Pt in starting solution (wt% Pt)	1	10	1	10	1	10
Adsorption rate (%)	~100.0	52.0	~100.0	51.4	~100.0	55.6
Amount of Pt loaded on CB (wt% Pt)	~1.00	5.20	~1.00	5.14	~1.00	5.56

**Table S7. The Number of Transferred Electrons for Each Catalyst at Diffusion-Limited Region**

Cluster	Pt <sub>-35</sub> /CB		Pt <sub>-51</sub> /CB		Pt <sub>-66</sub> /CB		Pt <sub>NP</sub> /CB
	without calcination	after calcination	without calcination	after calcination	without calcination	after calcination	
The number of electrons	3.5	3.7	3.8	4.0	4.0	4.1	4.3

## 7. Additional Figures

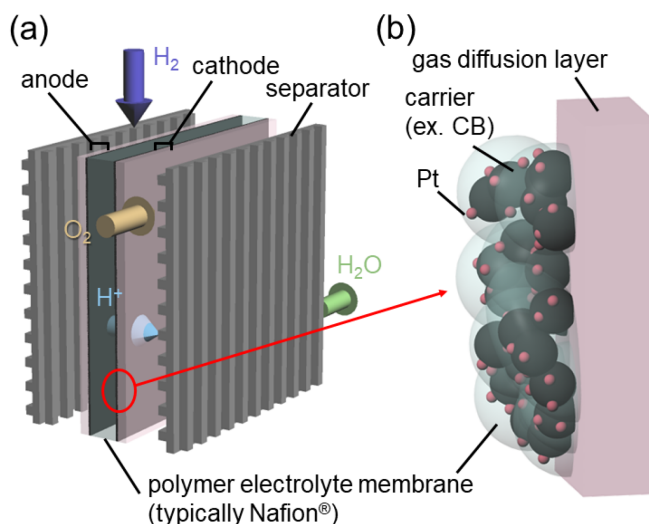


**Figure S1.** Schematic of a polymer electrolyte fuel cell (PEFC); (a) complete cell and (b) expanded version of cathode.<sup>19</sup>

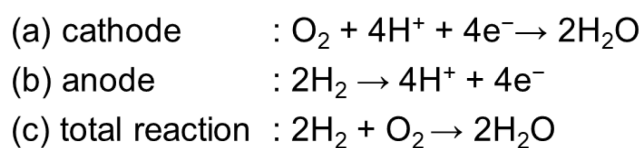


**Figure S2.** Reaction equations at (a) the cathode, (b) the anode, and (c) overall reaction.

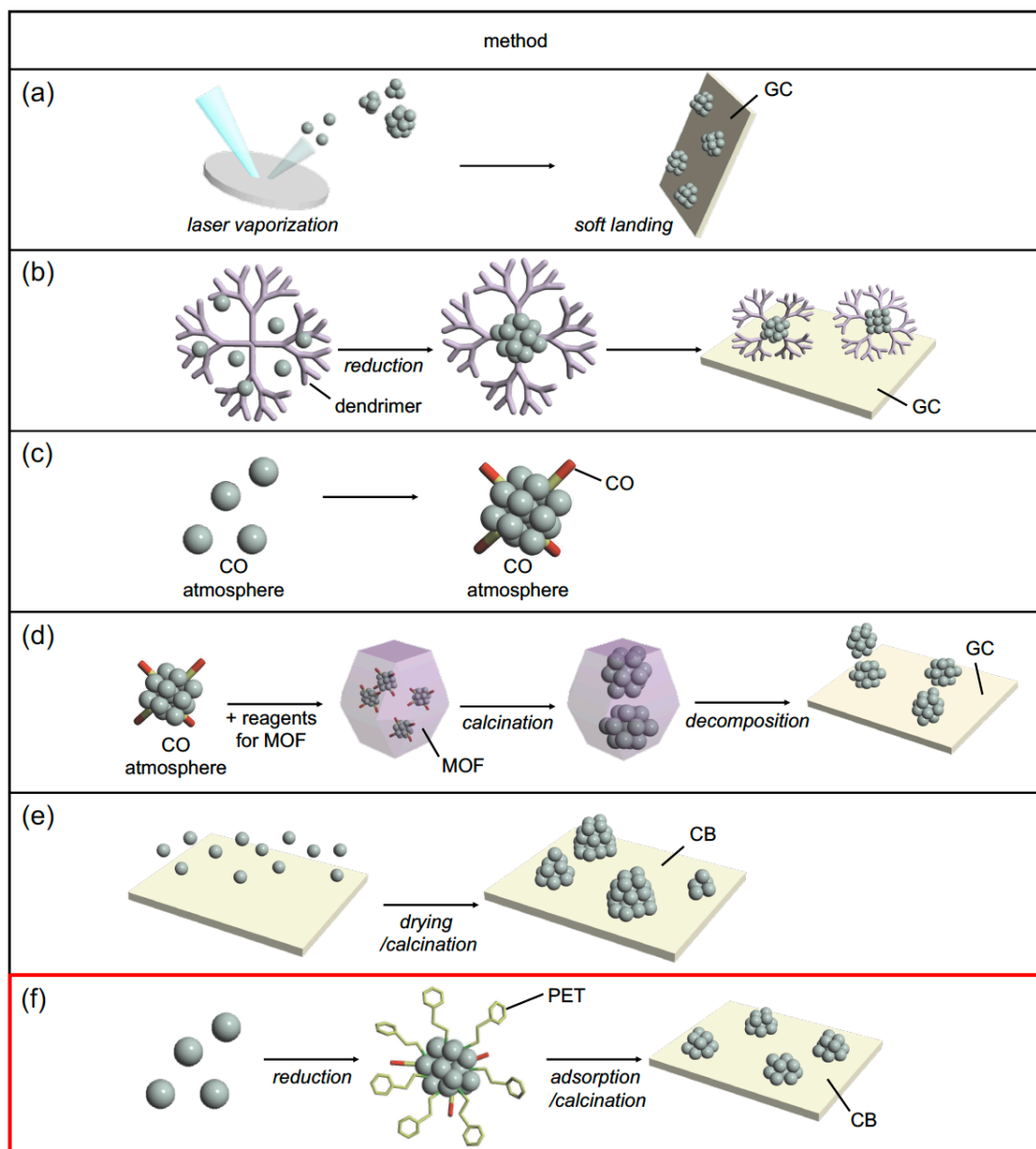


**Figure S3.** Comparison of formation, synthesis or preparation method of ~1 nm Pt NCs: (a) laser vaporization (or ion spattering) of bulk Pt under vacuum;<sup>20</sup> (b) synthesis using a specific dendrimer as a template;<sup>21</sup> (c) synthesis using CO as a ligand;<sup>22</sup> (d) synthesis in the metal-organic frameworks (MOF);<sup>23</sup> (e) aggregation of Pt atoms on the support by impregnation (or photoreduction) methods;<sup>24</sup> and (f) synthesis and thereafter loading of controlled Pt NCs on support (this work).<sup>25</sup> The substrates in this figure are either glassy carbon (GC) or carbon black (CB).

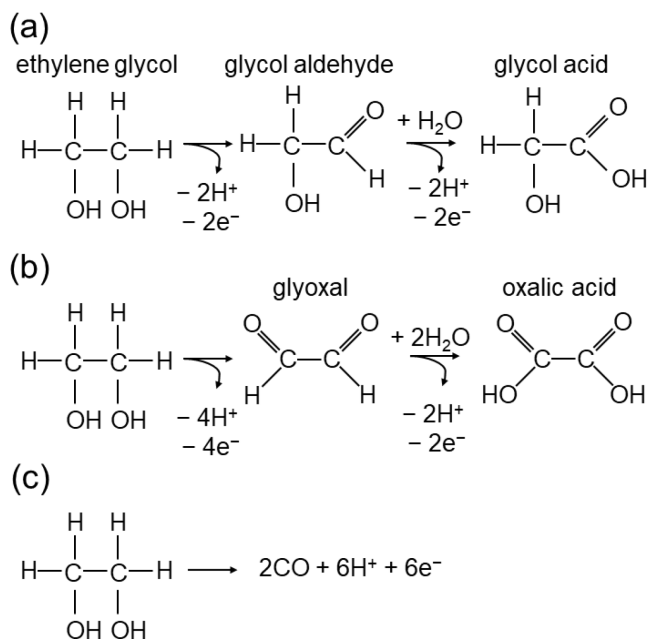


**Figure S4.** Proposed three schemes for oxidation of ethylene glycol, which is the reaction that delivers the required electrons for the reduction of the metal precursors (polyol-reduction method).<sup>26,27</sup> The oxidation of ethylene glycol can proceed via three different reaction pathways (a-c). CO is produced in reaction (c) and the resultant CO is considered to coordinate to the surface of metal NCs produced by polyol reduction.

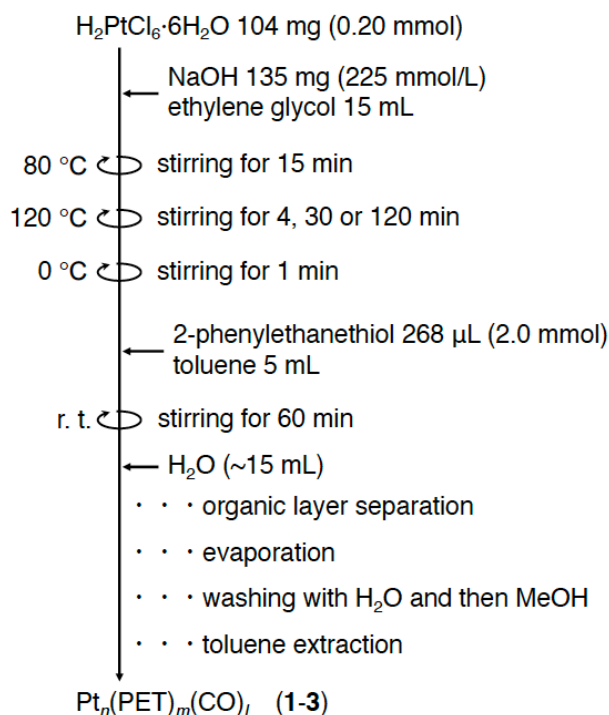


**Figure S5.** Protocol of the synthesis of 1-3.



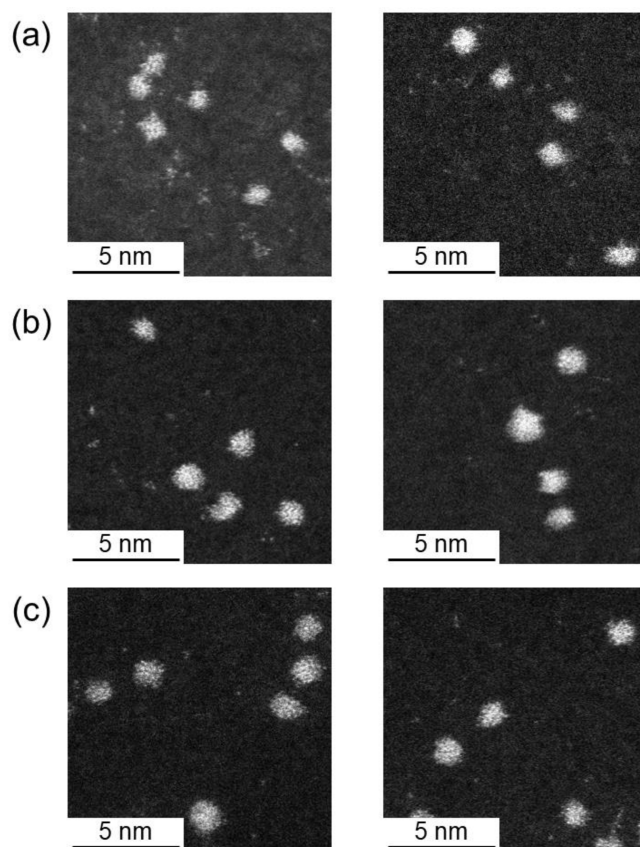


Fig. S7 Representative HAADF-STEM images of (a) 1, (b) 2, and (c) 3.

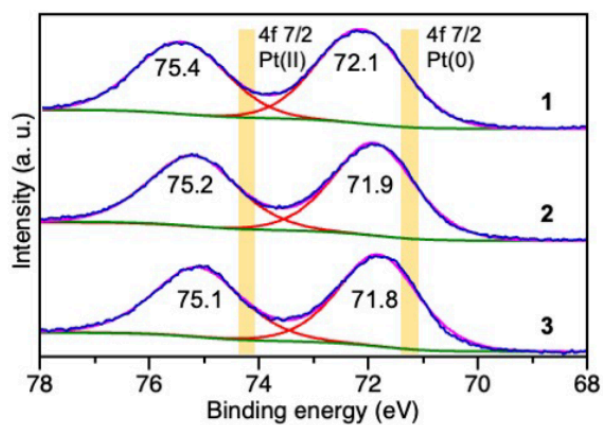
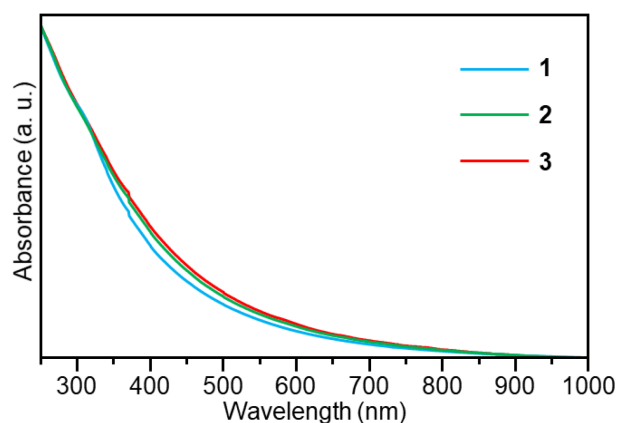
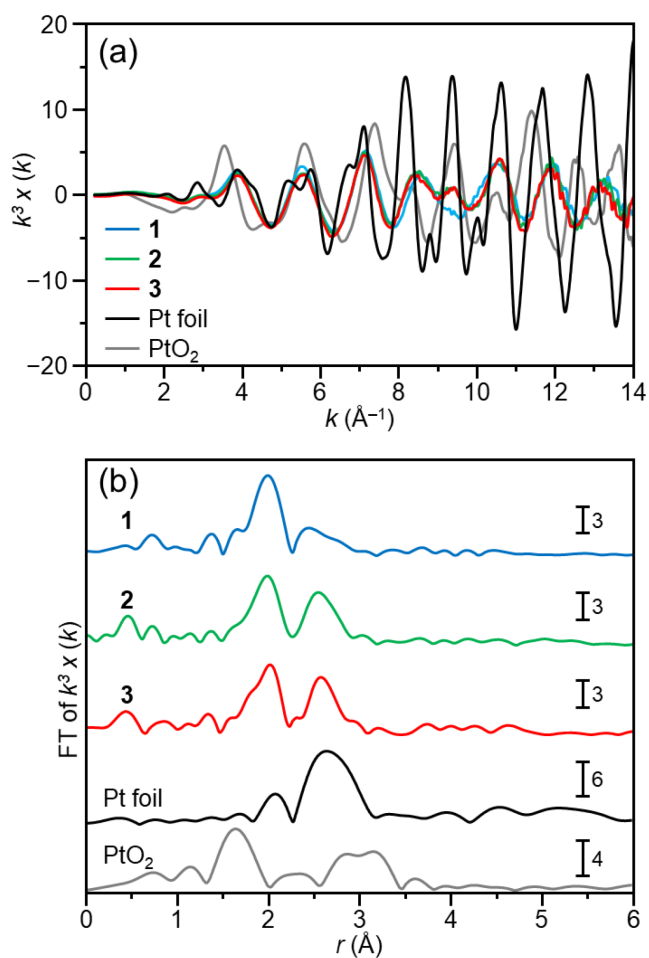


Figure S8. Pt 4f<sub>7/2</sub> XPS spectra (blue line) and their fitting results (red, green, and magenta lines) for 1–3. In this figure, yellow vertical lines indicate the position of Pt(0) and Pt(II).<sup>29</sup> These spectra indicate that 1–3 consist of the reduced Pt atoms, although the peak positions are slightly shifted to the higher binding energy side (oxidation side) compared to that of Pt surface due to the bonding with S.



**Figure S9.** Ultraviolet-visible absorption spectra of 1–3 in dichloromethane solution. The absorption in the region from visible to near infrared implies that 1–3 include the reduced Pt(0) atoms.



**Figure S10.** Results of Pt L<sub>3</sub>-edge (a) EXAFS and (b) FT-EXAFS for 1–3 together with Pt foil and PtO<sub>2</sub>. In (b), the peak at 2.2–3.0 Å is assigned to the Pt–Pt bond.<sup>30</sup> The existence of the peak in this region of the spectra shows that 1–3 include the reduced Pt(0) atoms.

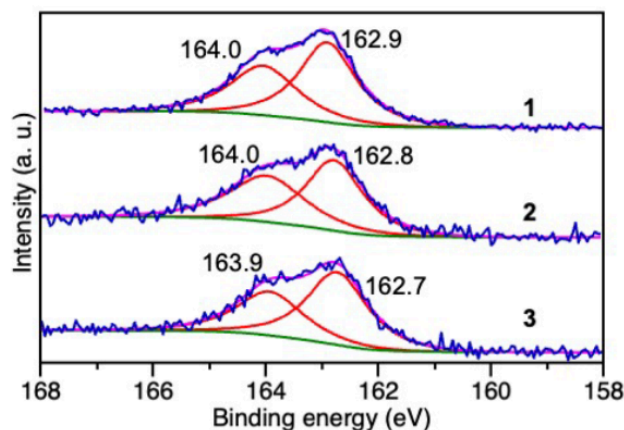


**Figure S11.** S 2p XPS spectra (blue line) and their fitting results (red, green, and magenta lines) for 1–3. These spectra indicate that 1–3 include the PET.

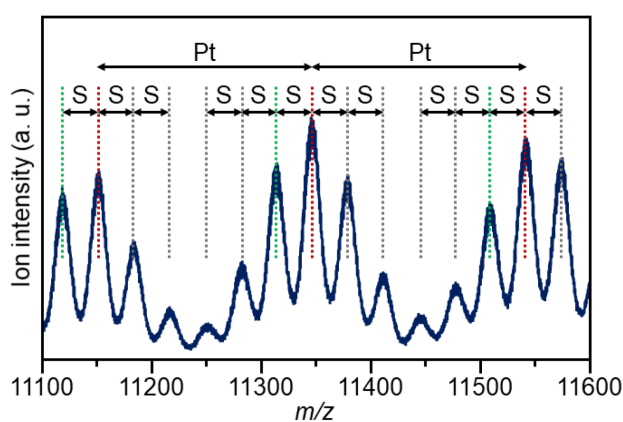


**Figure S12.** Expanded MALDI-MS spectrum of **2** (Figure 3a). The observed progression is caused by the distribution of the number of Pt and S atoms. This type of progression has often been observed for thiolate-protected gold NCs and interpreted to be caused by S–C dissociation due to laser irradiation.<sup>7–12</sup> This MS spectrum implies that a similar S–C dissociation also occurred for **2**. Similar results were also observed for **1** and **3**.

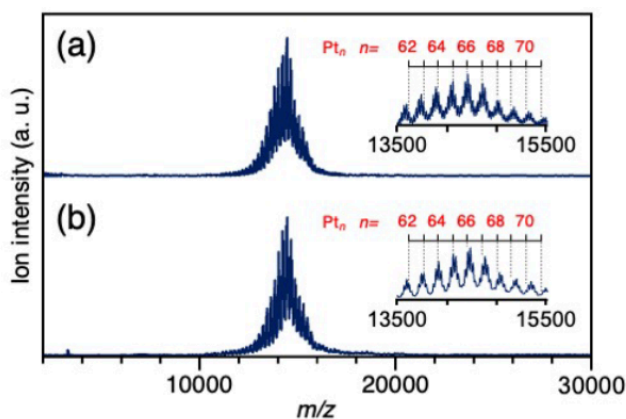


**Figure S13.** Comparison of MALDI-MS spectra between (a) **3** and (b) Pt<sub>66</sub> NCs protected by octanethiolate (OcT) and CO. The latter was synthesized with a similar protocol as **3** except using octanethiol instead of 2-phenylethanethiol for comparison purpose. Both spectra showed a similar mass distribution regardless of the different functional group (i.e. PET or OcT), thus supporting the interpretation that S–C dissociation also occurred for **3** (Figure S12).

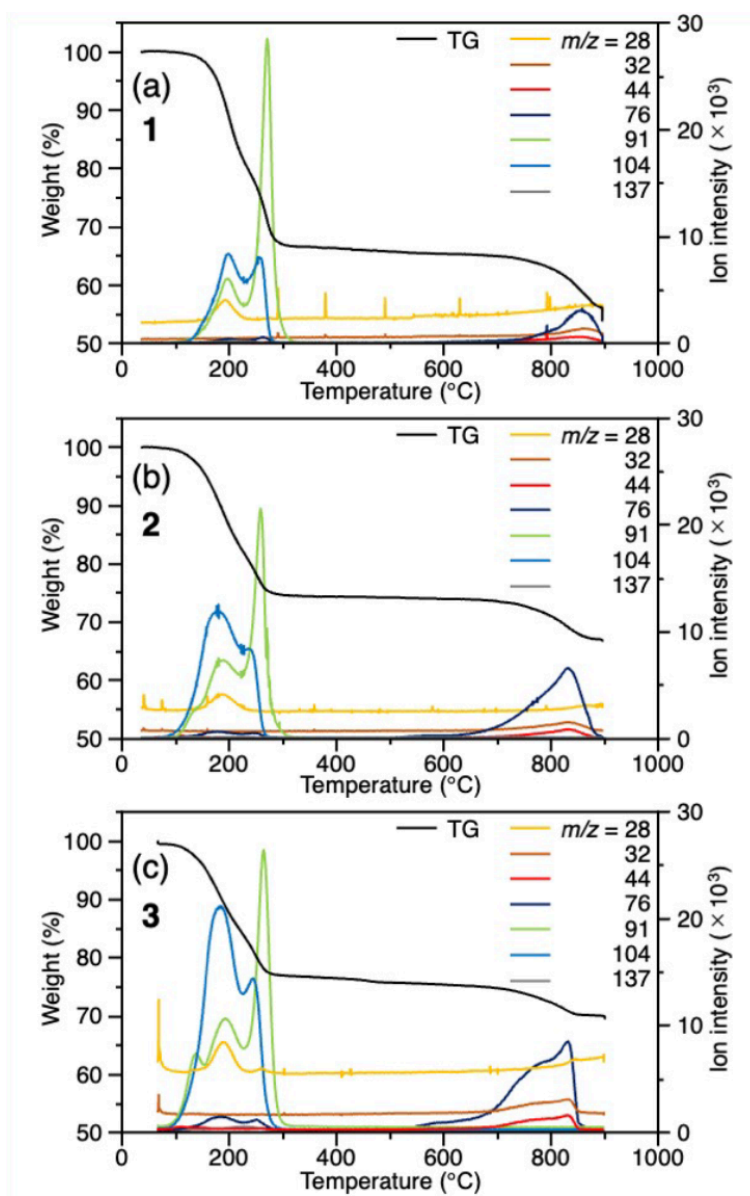


**Figure S14.** TG-MS spectra of (a) **1**, (b) **2**, and (c) **3** together with the TGA curves. The ion currents observed at  $m/z = 91$  ( $\text{PhCH}_2$ ) and  $104$  ( $\text{PhC}_2\text{H}_3$ ) are considered to originate from the S-C dissociation of PET. The ion currents observed at  $m/z = 28$  (CO),  $32$  (S),  $44$  ( $\text{CO}_2$ ), and  $76$  ( $\text{CS}_2$ ) are considered to relate to the desorption of CO and S ( $\text{CS}_2$  seems to be formed from CO and S on the surface of Pt NCs heated at high temperature). These results demonstrate that  $300\text{ }^\circ\text{C}$  is needed for all the S-C bond dissociation and  $900\text{ }^\circ\text{C}$  is needed for the complete elimination of all the ligands. On the basis of these results, Pt-<sub>35</sub>/CB, Pt-<sub>51</sub>/CB, and Pt-<sub>66</sub>/CB prepared by the calcination at  $200\text{ }^\circ\text{C}$  partly includes ligands on the surface. This interpretation is also consistent with the results from HAADF-STEM (Figure S16) and Pt L<sub>3</sub>-edge FT-EXAFS (Figure 5d).

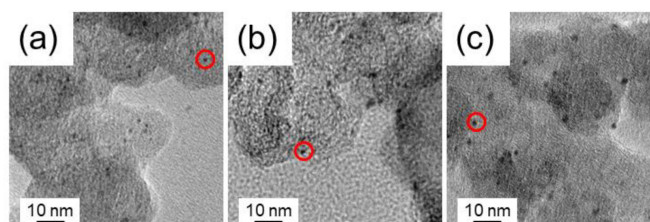


**Figure S15.** TEM images of (a) Pt-<sub>35</sub>/CB, (b) Pt-<sub>51</sub>/CB, and (c) Pt-<sub>66</sub>/CB before calcination, showing that there is almost no aggregation of the ligand-protected Pt<sub>n</sub> NCs on CB.

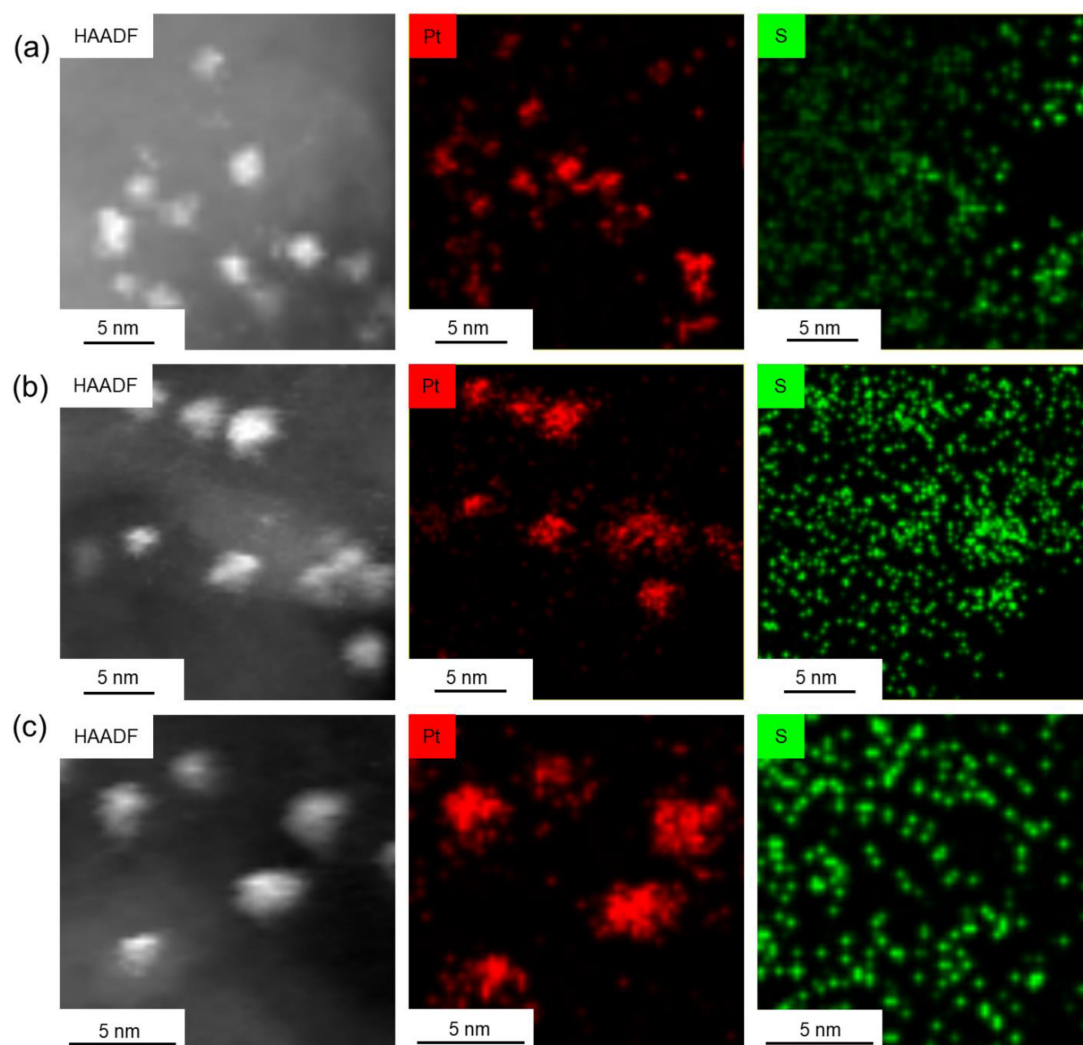


**Figure S16.** Representative HAADF-STEM images and elemental mapping (Pt and S) of (a) Pt-<sub>35</sub>/CB, (b) Pt-<sub>51</sub>/CB, and (c) Pt-<sub>66</sub>/CB. The results indicate that S remains on the surface of Pt and CB,<sup>31</sup> at least before the electrochemical cleaning.

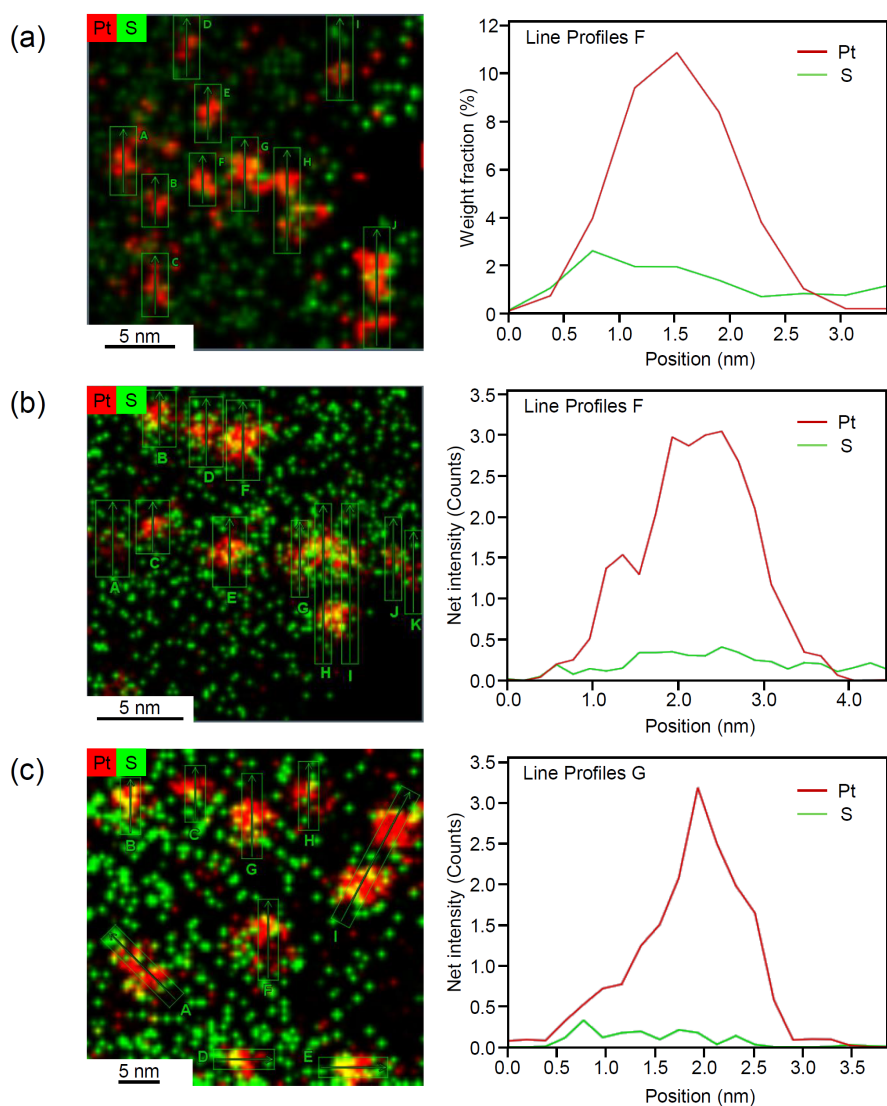


**Figure S17.** Line-analyses obtained from HAADF-STEM images for Pt and S; (a) Pt-<sub>35</sub>/CB, (b) Pt-<sub>51</sub>/CB, and (c) Pt-<sub>66</sub>/CB. The results indicate that S remains on the surface of Pt and CB,<sup>31</sup> at least before the electrochemical cleaning.

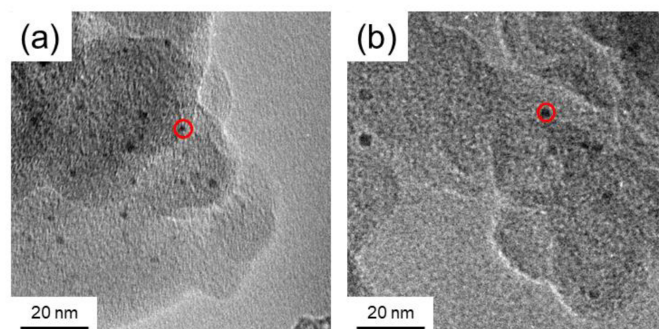


**Figure S18.** TEM images of Pt-<sub>66</sub>/CB calcined at (a) 250 °C ( $2.0 \pm 0.4$  nm) and (b) 300 °C ( $2.1 \pm 0.5$  nm). In the obtained catalysts, a little aggregation of Pt-<sub>66</sub> was observed.

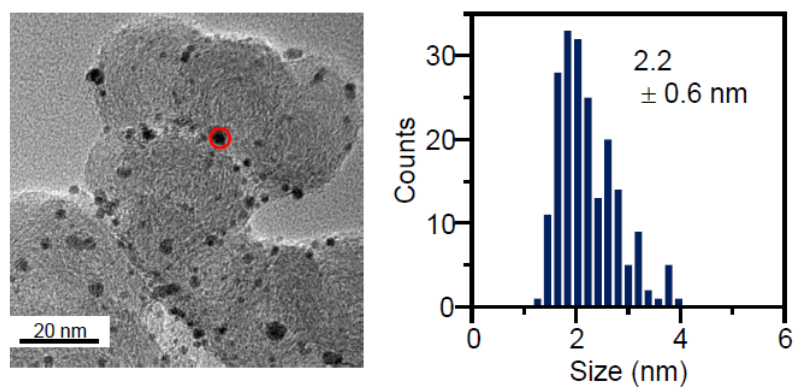


**Figure S19.** TEM images of the commercial Pt NPs/CB (13 wt% Pt). The average particle size was estimated to be  $2.6 \pm 0.6$  nm from the histogram (inset).

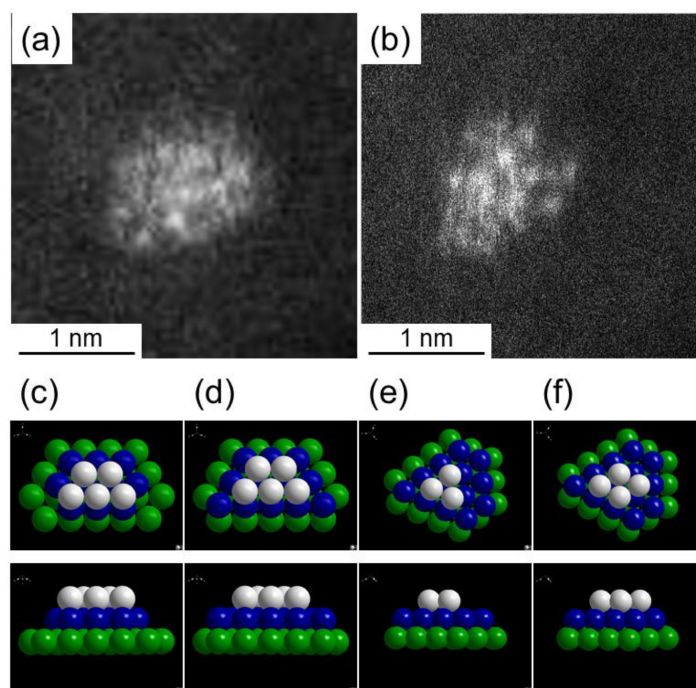


**Figure S20.** (a, b) Expanded HAADF-STEM images of Pt<sub>35</sub> supported on CB showing two different morphologies. (c–f) Estimated geometrical structures of Pt<sub>35</sub> supported on CB; the structures (c, d) correspond to the HAADF-STEM (a), whereas the structures (e, f) correspond to the HAADF-STEM (b). In (c–f), both top- and side-angle structures are shown.

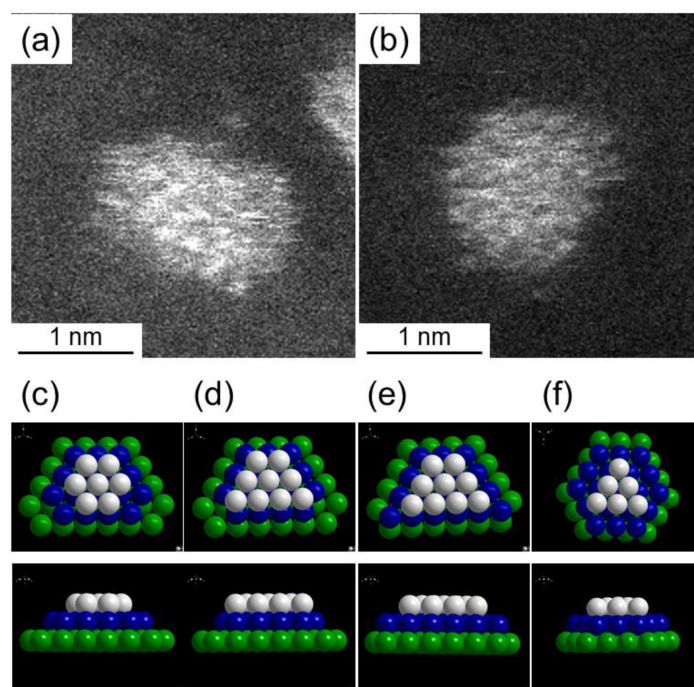


**Figure S21.** (a, b) Expanded HAADF-STEM images of Pt<sub>51</sub> supported on CB showing two different morphologies. (c–f) Estimated geometrical structures of Pt<sub>51</sub> supported on CB; the structures (c–e) correspond to the HAADF-STEM (a), whereas the structure (f) corresponds to the HAADF-STEM (b). In (c–f), both top- and side-angle structures are shown.

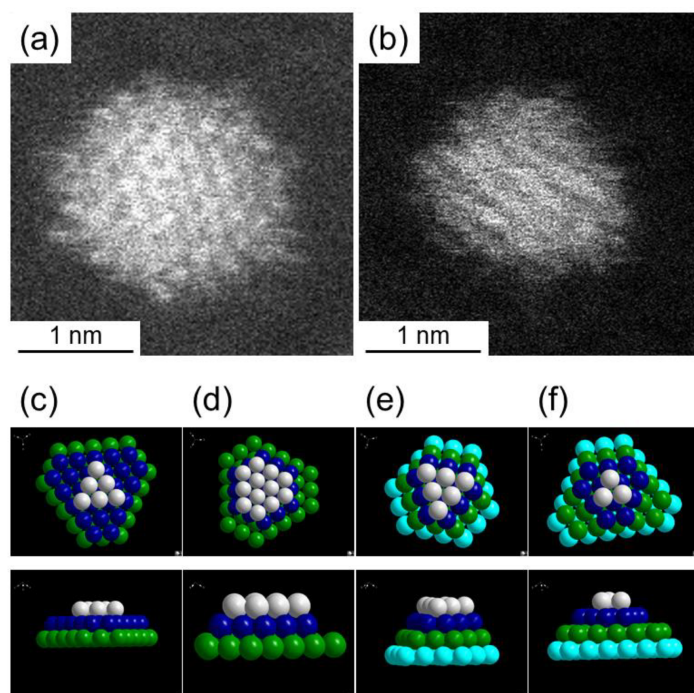


**Figure S22.** (a, b) Expanded HAADF-STEM images of Pt<sub>66</sub> supported on CB showing two different morphologies. (c–f) Estimated geometrical structures of Pt<sub>66</sub> supported on CB; the structures (c, d) correspond to the HAADF-STEM (a), whereas the structures (e, f) correspond to the HAADF-STEM (b). In (c–f), both top- and side-angle structures are shown.

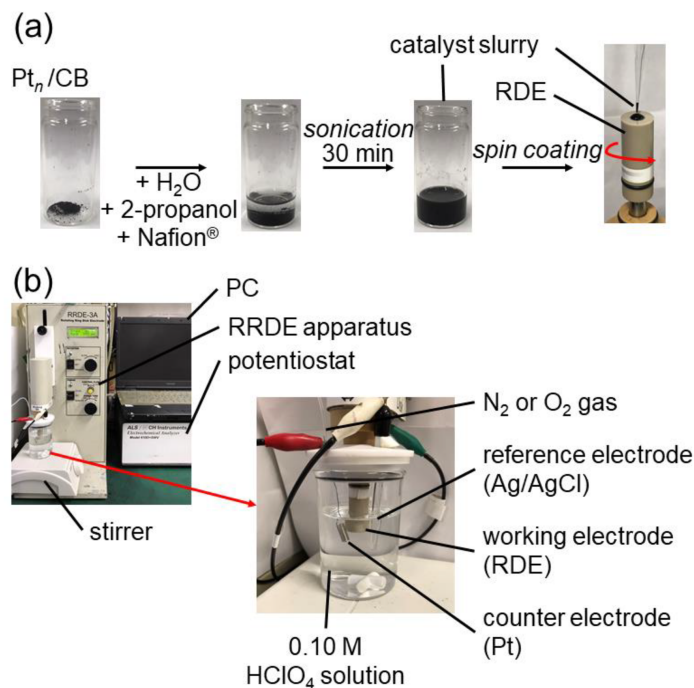


**Figure S23.** Schematic of setup of electrochemical experiment: (a) preparation of Pt<sub>n</sub>/CB catalyst slurry and their loading on RDE; (b) photographs of the apparatus used in this work.

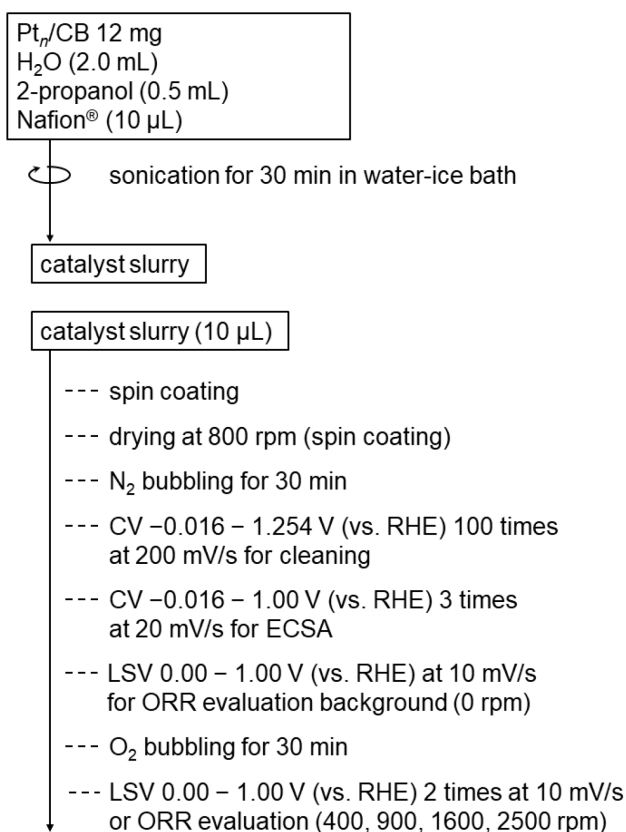


**Figure S24.** Protocol for the preparation of Pt<sub>n</sub>/CB catalyst slurry and electrochemical measurements (CV and LSV curves) used in this work.

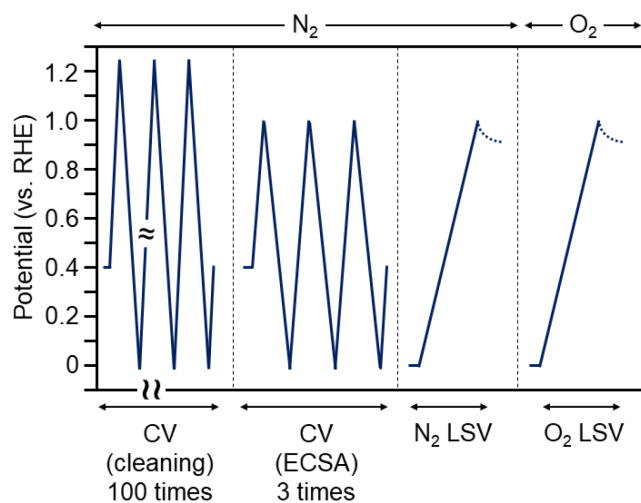


**Figure S25.** Flow of the electrochemical measurements (CV and LSV curves) used in this work.

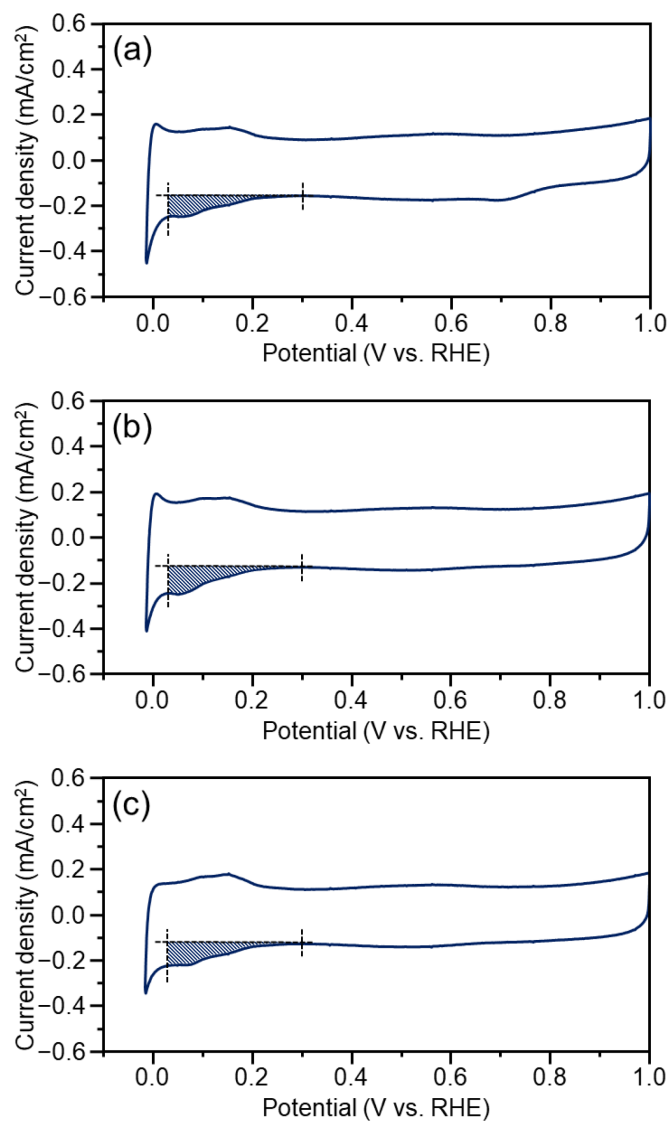


**Figure S26.** CV curves obtained for (a) Pt-<sub>35</sub>/CB (1.00 wt% Pt), (b) Pt-<sub>51</sub>/CB (1.00 wt% Pt), and (c) Pt-<sub>66</sub>/CB (1.00 wt% Pt). The shadow areas originate from the hydrogen adsorption.<sup>32</sup> ECSA of each catalyst (top of Figure 6a) was estimated based on this area.

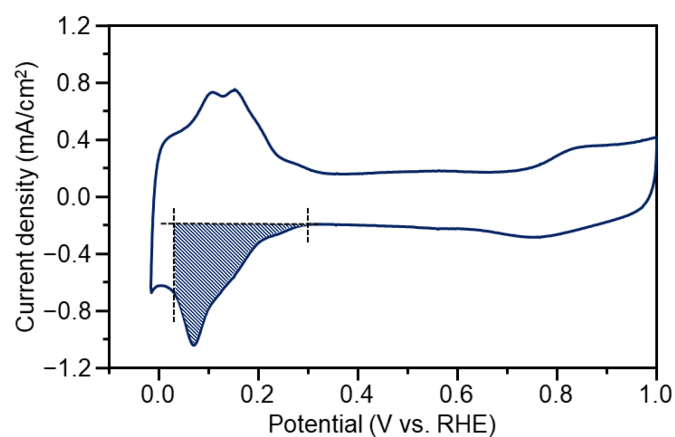


**Figure S27.** CV curve obtained for the commercial Pt NPs/CB (13 wt% Pt; Fig. S18). The shadow area originates from the hydrogen adsorption.<sup>32</sup> ECSA of catalyst (top of Figure 6a) was estimated based on this area.

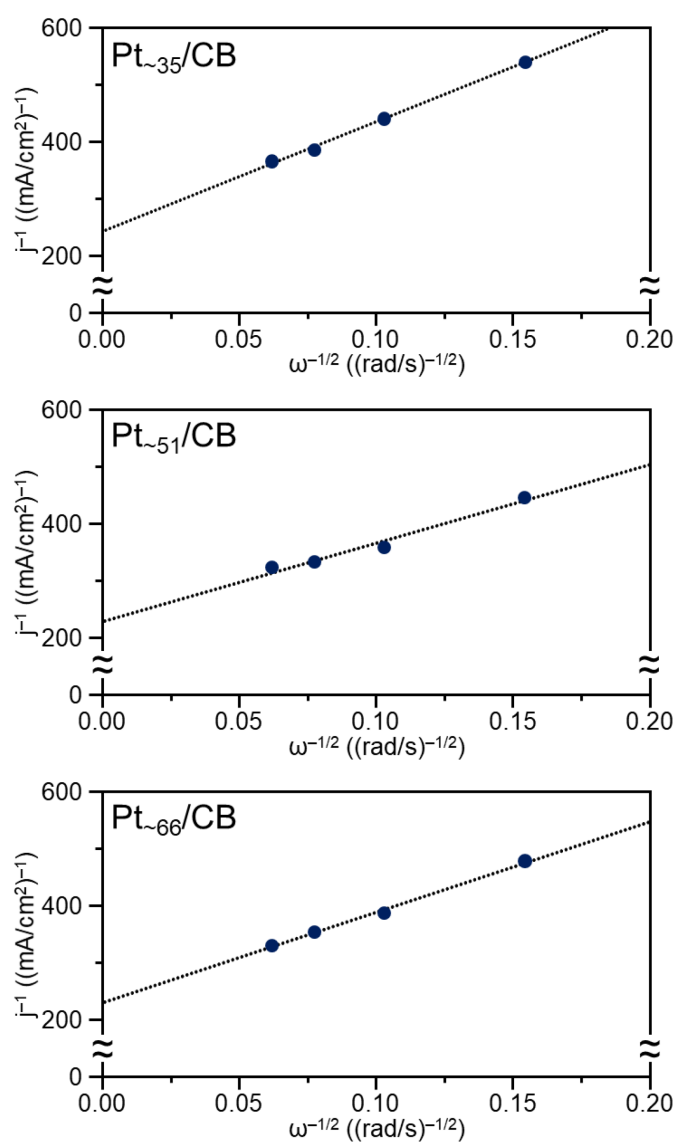


**Figure S28.** Koutecky-Levich plots<sup>33</sup> for Pt<sub>35</sub>/CB (1.00 wt% Pt), Pt<sub>51</sub>/CB (1.00 wt% Pt), and Pt<sub>66</sub>/CB (1.00 wt% Pt). The number of the transferred electrons (Table S7) and the mass activity (middle of Figure 6a) were calculated on the basis of these results.

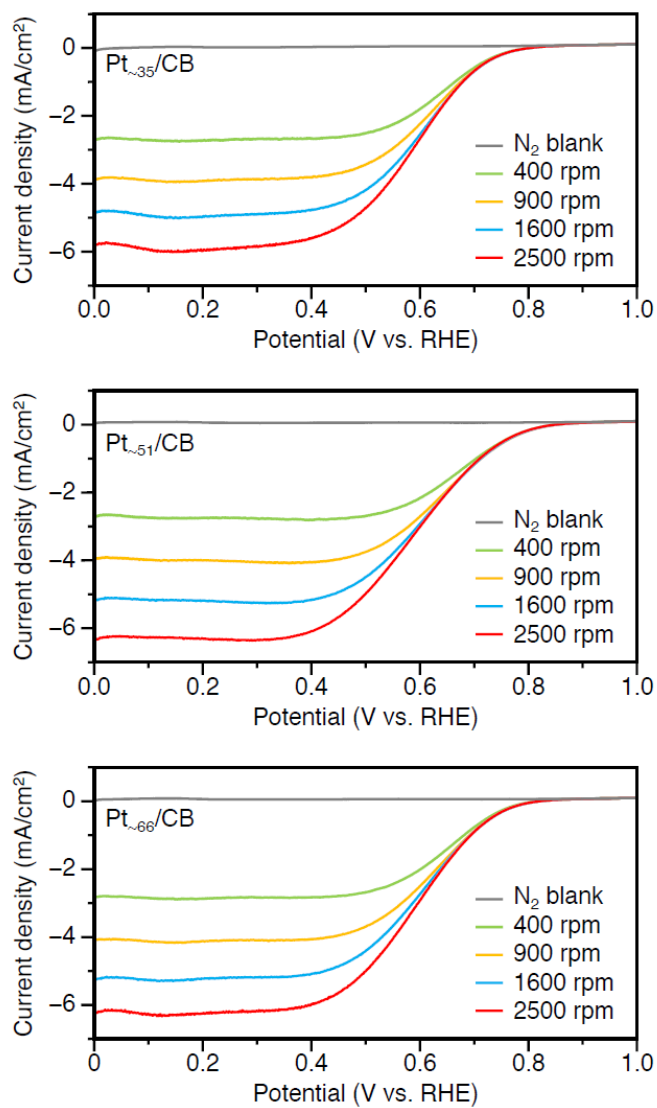


**Figure S29.** Comparison of LSV curves for (top) Pt<sub>35</sub>/CB, (middle) Pt<sub>51</sub>/CB, and (bottom) Pt<sub>66</sub>/CB obtained for electrode rotation speeds of 400–2500 rpm under O<sub>2</sub> gas. The measurements under N<sub>2</sub> gas were conducted for baseline comparison.

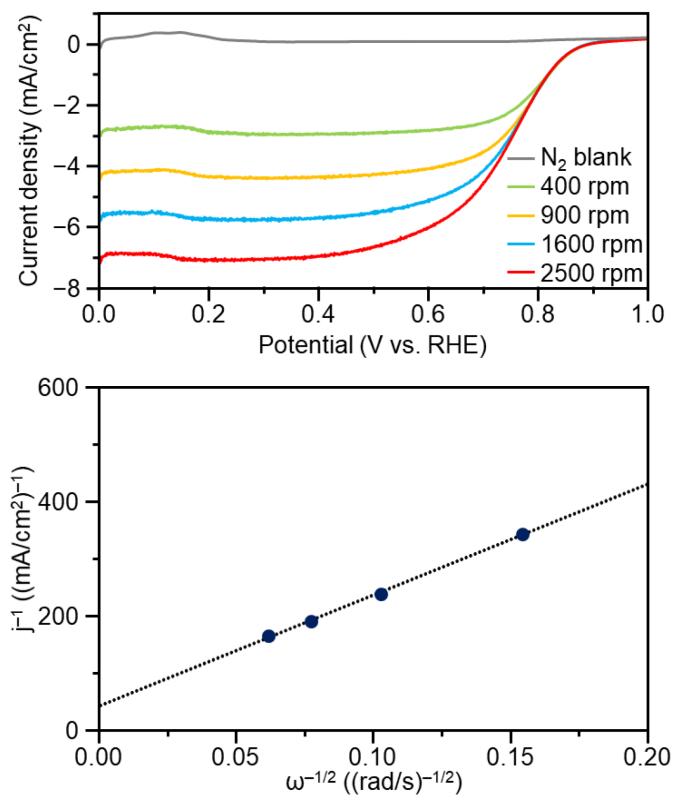


**Figure S30.** (a) LSV curves obtained for the commercial Pt<sub>NP</sub>/CB (13 wt% Pt; Figure S18) at an electrode rotation speed of 400–2500 rpm under O<sub>2</sub> gas. The measurement under N<sub>2</sub> gas was conducted for comparison. (b) Koutecky-Levich plots<sup>33</sup> obtained for commercial Pt<sub>NP</sub>/CB (13 wt% Pt). The number of transferred electrons (Table S7) and the mass activity (middle of Figure 6a) were calculated on the basis of this result.

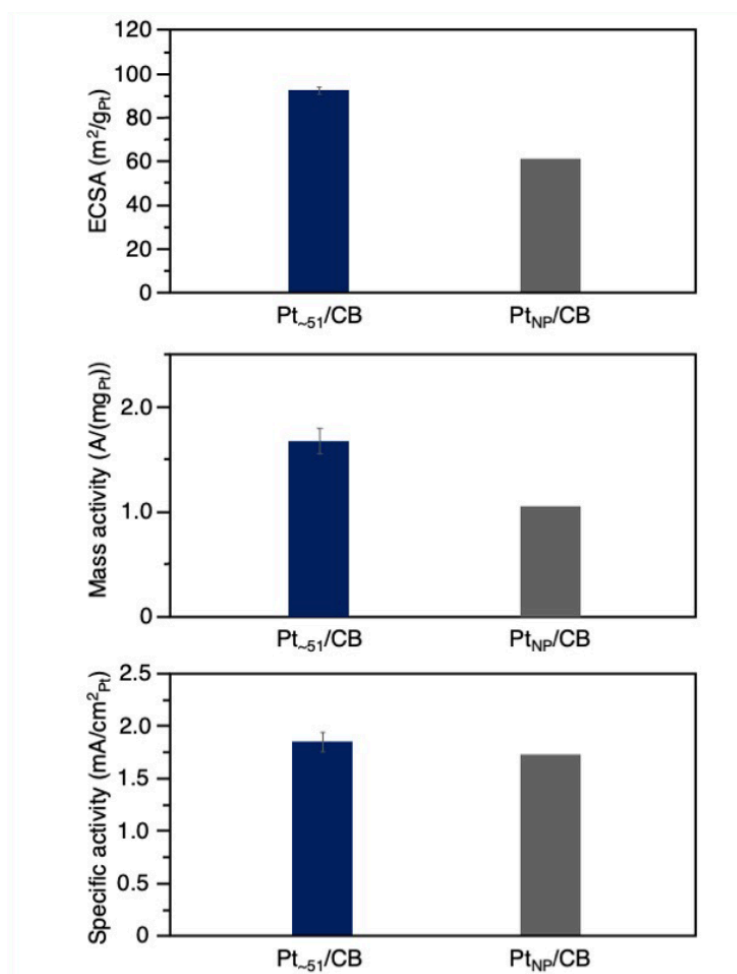


**Figure S31.** Comparison of (a) ECSA, (b) ORR mass activity at 0.6 V vs. RHE, and (c) ORR specific activity between Pt<sub>-51</sub>/CB (5.1 wt% Pt; Table S6) and Pt<sub>NP</sub>/CB (6.5 wt% Pt). The Pt<sub>NP</sub>/CB (6.5 wt% Pt) was prepared by adding the CB to the commercial Pt<sub>NP</sub>/CB (13 wt% Pt). In these figures, the average value over 3 times experiments are described for Pt<sub>-51</sub>/CB (5.1 wt% Pt).

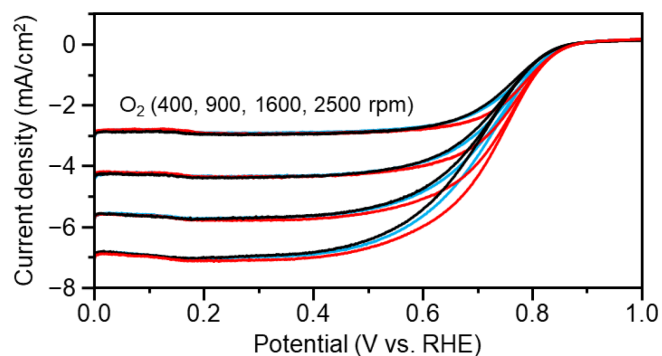


**Figure S32.** Comparison of LSV curves between Pt<sub>51</sub>/CB (5.14 wt% Pt (Table S6); cyan), Pt<sub>66</sub>/CB (5.56 wt% Pt (Table S6); red), and commercial Pt<sub>NP</sub>/CB (6.5 wt% Pt; black). These curves were obtained by the LSV at a rotating rate of 400, 900, 1600, and 2500 rpm under O<sub>2</sub> atmosphere (the baseline obtained by LSV under N<sub>2</sub> atmosphere are subtracted from these curves). These results indicate that the overpotential is lower for Pt<sub>51</sub>/CB and Pt<sub>66</sub>/CB compared with the commercial Pt<sub>NP</sub>/CB.

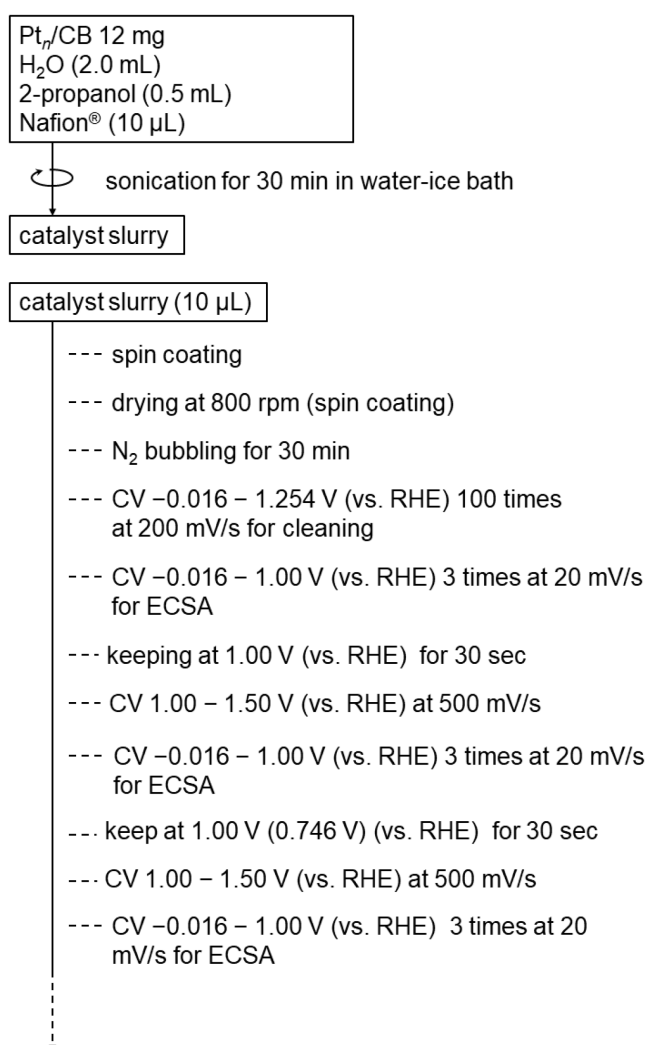


**Figure S33.** Protocol of the durability test used in this work.<sup>20</sup>

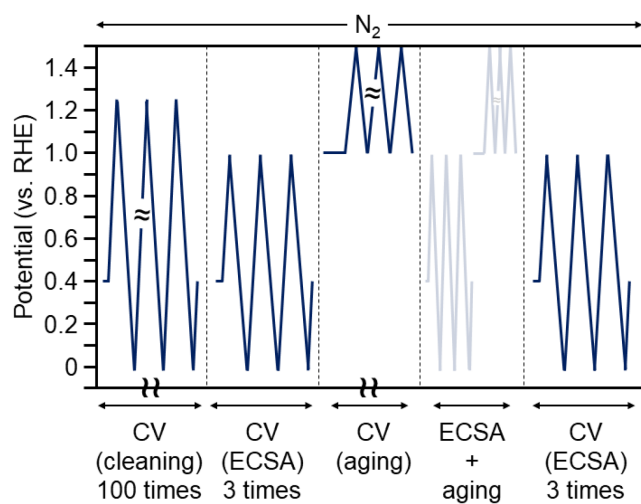


**Figure S34.** Flow of the durability test used in this work.<sup>20</sup>

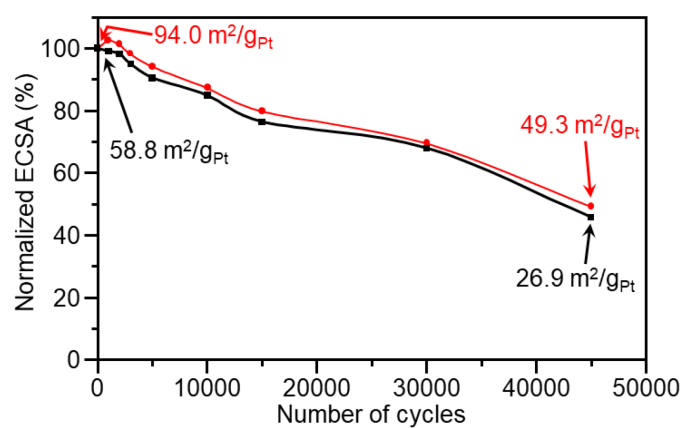


**Figure S35.** Normalized ECSA of Pt<sub>-66</sub>/CB (red) and commercial Pt<sub>NP</sub>/CB (black) during accelerated durability test. In this experiment, Pt<sub>-66</sub> with 5.6 wt% Pt (Table S6) and Pt<sub>NP</sub>/CB with 6.5 wt% Pt were used since the large difference in loading weigh might affect the durability of the catalysts. The values of the actual ECSA before and after the durability test are also shown in this figure.

## 8. References

- [1] L. V. Nair, S. Hossain, S. Wakayama, S. Takagi, M. Yoshioka, J. Maekawa, A. Harasawa, B. Kumar, Y. Niihori, W. Kurashige, Y. Negishi, *J. Phys. Chem. C* **2017**, *121*, 11002–11009.
- [2] Y. Negishi, N. Shimizu, K. Funai, R. Kaneko, K. Wakamatsu, A. Harasawa, S. Hossain, M. E. Schuster, D. Ozkaya, W. Kurashige, T. Kawawaki, S. Yamazoe, S. Nagaoka, *Nanoscale Adv.* **2020**, *2*, 669–678.
- [3] D. Rivin, *Rubber Chem. Technol.* **1971**, *44*, 307–343.
- [4] H. Asakura, S. Yamazoe, T. Misumi, A. Fujita, T. Tsukuda, T. Tanaka, *Radiat. Phys. Chem.* **2020**, *175*, 108270.
- [5] Y. Garsany, I. L. Singer, K. E. Swider-Lyons, *J. Electroanal. Chem.* **2011**, *662*, 396–406.
- [6] A. Ohma, K. Shinohara, A. Iiyama, T. Yoshida, A. Daimaru, *ECS Trans.* **2011**, *41*, 775–784.
- [7] Y. Negishi, K. Nobusada, T. Tsukuda, *J. Am. Chem. Soc.* **2005**, *127*, 5261–5270.
- [8] Z. Wu, R. Jin, *ACS Nano* **2009**, *3*, 2036–2042.
- [9] N. K. Chaki, Y. Negishi, H. Tsunoyama, Y. Shichibu, T. Tsukuda, *J. Am. Chem. Soc.* **2008**, *130*, 8608–8610.
- [10] H. Tsunoyama, Y. Negishi, T. Tsukuda, *J. Am. Chem. Soc.* **2006**, *128*, 6036–6037.
- [11] H. Qian, R. Jin, *Nano Lett.* **2009**, *9*, 4083–4087.
- [12] T. G. Schaaff, M. N. Shafiqullin, J. T. Khoury, I. Vezmar, R. L. Whetten, *J. Phys. Chem. B* **2001**, *105*, 8785–8796.
- [13] N. M. Marković, H. A. Gasteiger, B. N. Grgur, P. N. Ross, *J. Electroanal. Chem.* **1999**, *467*, 157–163.
- [14] E. Cattabriga, I. Ciabatti, C. Femoni, T. Funaioli, M. C. Iapalucci, S. Zacchini, *Inorg. Chem.* **2016**, *55*, 6068–6079.
- [15] J. Koivisto, K. Salorinne, S. Mustalahti, T. Lahtinen, S. Malola, H. Häkkinen, M. Pettersson, *J. Phys. Chem. Lett.* **2014**, *5*, 387–392.
- [16] H. M. Badawi, *Spectrochim. Acta, Part A* **2011**, *82*, 63–68.
- [17] M. Farrag, M. Tschurl, A. Dass, U. Heiz, *Phys. Chem. Chem. Phys.* **2013**, *15*, 12539–12542.
- [18] A. J. Bard, L. R. Faulkner, *Electrochemical methods: Fundamentals and applications*, J. Wiley and Sons, New York, **2001**.
- [19] R. Borup, J. Meyers, B. Pivovar, Y. S. Kim, R. Mukundan, N. Garland, D. Myers, M. Wilson, F. Garzon, D. Wood, P. Zelenay, K. More, K. Stroh, T. Zawodzinski, J. Boncella, J. E. McGrath, M. Inaba, K. Miyatake, M. Hori, K. Ota, Z. Ogumi, S. Miyata, A. Nishikata, Z. Siroma, Y. Uchimoto, K. Yasuda, K.-i. Kimijima, N. Iwashita, *Chem. Rev.* **2007**, *107*, 3904–3951.
- [20] A. von Weber, S. L. Anderson, *Acc. Chem. Res.* **2016**, *49*, 2632–2639.
- [21] K. Yamamoto, T. Imaoka, W.-J. Chun, O. Enoki, H. Katoh, M. Takenaga, A. Sono, *Nat. Chem.* **2009**, *1*, 397–402.
- [22] I. Ciabatti, C. Femoni, M. C. Iapalucci, S. Ruggieri, S. Zacchini, *Coord. Chem. Rev.* **2018**, *355*, 27–38.
- [23] B. Garlyyev, K. Kratzl, M. Rück, J. Michalička, J. Fichtner, J. M. Macak, T. Kratky, S. Günther, M. Cokoja, A. S. Bandarenka, A. Gagliardi, R. A. Fischer, *Angew. Chem., Int. Ed.* **2019**, *58*, 9596–9600.
- [24] X. Hao, L. Quach, J. Korah, W. A. Spieker, J. R. Regalbutto, *J. Mol. Catal. A: Chem.* **2004**, *219*, 97–107.
- [25] Y. Negishi, N. Shimizu, K. Funai, R. Kaneko, K. Wakamatsu, A. Harasawa, S. Hossain, M. E. Schuster, D. Ozkaya, W. Kurashige, T. Kawawaki, S. Yamazoe, S. Nagaoka, *Nanoscale Adv.* **2020**, *2*, 669–678.
- [26] C. Bock, C. Paquet, M. Couillard, G. A. Botton, B. R. MacDougall, *J. Am. Chem. Soc.* **2004**, *126*, 8028–8037.
- [27] I. Schrader, J. Warneke, S. Neumann, S. Grotheer, A. A. Swane, J. J. K. Kirkensgaard, M. Arenz, S. Kunz, *J. Phys. Chem. C* **2015**, *119*, 17655–17661.
- [28] T. Ikeda, A. Xiong, T. Yoshinaga, K. Maeda, K. Domen, T. Teranishi, *J. Phys. Chem. C* **2013**, *117*, 2467–2473.
- [29] R. Badam, R. Vedarajan, K. Okaya, K. Matsutani, N. Matsumi, *Sci. Rep.* **2016**, *6*, 37006.
- [30] T. Imaoka, Y. Akanuma, N. Haruta, S. Tsuchiya, K. Ishihara, T. Okayasu, W.-J. Chun, M. Takahashi, K. Yamamoto, *Nat. Commun.* **2017**, *8*, 688.
- [31] B. Zhang, A. Sels, G. Salassa, S. Pollitt, V. Truttmann, C. Rameshan, J. Llorca, W. Olszewski, G. Rupprechter, T. Bürgi, N. Barrabés, *ChemCatChem* **2018**, *10*, 5372–5376.
- [32] K. J. J. Mayrhofer, D. Strmcnik, B. B. Blizanac, V. Stamenkovic, M. Arenz, N. M. Markovic, *Electrochim. Acta* **2008**, *53*, 3181–3188.
- [33] M. Li, Z. Zhao, T. Cheng, A. Fortunelli, C.-Y. Chen, R. Yu, Q. Zhang, L. Gu, B. V. Merinov, Z. Lin, E. Zhu, T. Yu, Q. Jia, J. Guo, L. Zhang, W. A. Goddard III, Y. Huang, X. Duan, *Science* **2016**, *354*, 1414–1419.